



## EDGE ARTICLE

[View Article Online](#)  
[View Journal](#) | [View Issue](#)Cite this: *Chem. Sci.*, 2022, 13, 11360 All publication charges for this article have been paid for by the Royal Society of Chemistry

## A platinum–ruthenium hybrid prodrug with multi-enzymatic activities for chemo-catalytic therapy of hypoxic tumors†

Gang-Gang Yang,<sup>ab</sup> Xu-Xian Su,<sup>a</sup> Bing-Bing Liang,<sup>a</sup> Zheng-Yin Pan,<sup>a</sup> Qian Cao <sup>\*a</sup> and Zong-Wan Mao <sup>\*a</sup>

Regulation of tumor hypoxia and redox homeostasis is a promising strategy for cancer therapy. Nanocatalytic medicine has played more and more important roles in this field because it can cleverly convert the efficiency and selectivity of catalysis into high therapeutic efficiency. Herein, we developed a platinum(IV)–ruthenium hybrid prodrug, named as Pt–Ru, for efficient chemo-catalytic synergistic therapy of hypoxic tumors. The ruthenium hybridization endowed the Pt(IV) prodrug with multi-enzyme catalytic activity, that is, mimicking catalase (CAT) to generate O<sub>2</sub> *in situ*, mimicking peroxidase (POD) to produce reactive oxygen species, and mimicking glutathione peroxidase (GPx) to deplete GSH, thus effectively overcoming tumor hypoxia and cisplatin resistance. As a result, Pt–Ru treatment led to a superior anticancer efficacy to cisplatin both *in vitro* and *in vivo*. This work suggested redox homeostasis regulation as a tantalizing angle for developing the next generation of platinum drugs.

Received 16th June 2022  
Accepted 14th August 2022

DOI: 10.1039/d2sc03375e

[rsc.li/chemical-science](http://rsc.li/chemical-science)

## Introduction

In recent years, the concept of “nanocatalytic medicine” has attracted extensive attention and played more and more important roles in the field of cancer therapy.<sup>1–3</sup> This emerging strategy cleverly converts the efficiency and selectivity of catalysis into high therapeutic efficiency with reduced side effects.<sup>4</sup> Compared with normal tissue cells, tumor cells metabolize in different ways to form a characteristic tumor microenvironment and redox homeostasis, thus making it possible to trigger catalytic therapy selectively in tumor cells and tissues.<sup>5,6</sup>

Hypoxia, characterized by a low oxygen concentration, is a prominent feature of a tumor microenvironment playing important roles in tumor recurrence, angiogenesis and metastasis.<sup>7–9</sup> Extensive evidence has demonstrated that hypoxia can seriously reduce the efficacy of chemotherapeutic drugs and induce multi-drug resistance in the treatment of solid tumors.<sup>10–12</sup> Therefore, chemotherapeutic drugs which can overcome tumor hypoxia are highly required. Cisplatin is one of the most widely used antitumor drugs in clinics, and continuous efforts are still being made to address these serious problems of cisplatin resistance and side effects.<sup>13–16</sup> Recently,

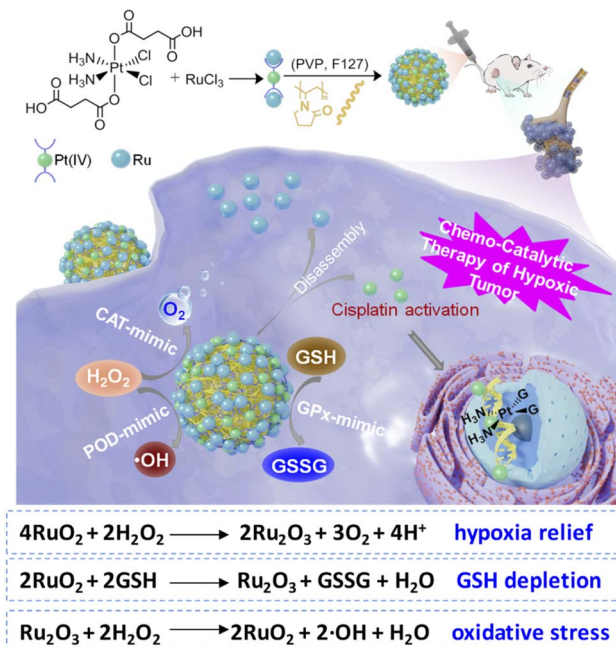
the nanocatalytic medicine strategy has been used to improve the efficacy of platinum drugs, especially against hypoxic tumors,<sup>17–19</sup> for example, co-delivery of catalase and Pt(II) drugs by poly(D,L-lactic-co-glycolic acid) nanoparticles, and encapsulation of catalase inside liposomes consisting of Pt(IV) prodrug-conjugated phospholipids, both realizing hypoxia relief by catalyzing endogenous hydrogen peroxide (H<sub>2</sub>O<sub>2</sub>) to generate oxygen.<sup>20,21</sup> Inorganic nanomaterials such as MnO<sub>2</sub> capable of mimicking catalase were also reported to enhance the efficacy of platinum drugs against hypoxic tumors *via* incorporation inside human serum protein (HSA) modified Pt(IV) prodrugs.<sup>22</sup> However, co-loading of platinum drugs and exogenous oxygen production catalysts may bring inevitable catalyst leakage and nanomaterial safety problems.<sup>23,24</sup> For this reason, we have recently designed a novel platinum(IV) prodrug, CAIXplatin, which can endogenously regulate oxygen contents by targeting and inhibiting carbonic anhydrase IX.<sup>17</sup>

Besides hypoxia, a high concentration of glutathione (GSH) in cancer cells (~10 mM) is a well-known cause of cisplatin resistance and detoxification, due to the extensive Pt–GSH conjugation and rapid export from cells *via* the glutathione S-conjugate pump.<sup>25–27</sup> Due to redox homeostasis, cancer cells also possess higher reactive oxygen species (ROS) levels than normal cells, meaning that cancer cells are more vulnerable to oxidative stress.<sup>28–30</sup> Inspired by these, development of multi-functional platinum drugs capable of alleviating hypoxia, consuming GSH, and promoting oxidative stress simultaneously should have profound significance in the clinical treatment of cancer. Considering that ruthenium complexes are the most likely substitutes for platinum drugs, some of which

<sup>a</sup>MOE Key Laboratory of Bioinorganic and Synthetic Chemistry, School of Chemistry, Sun Yat-Sen University, Guangzhou 510275, P. R. China. E-mail: caoqian3@mail.sysu.edu.cn; cesmzw@mail.sysu.edu.cn

<sup>b</sup>School of Chemistry and Chemical Engineering, Anhui University of Technology, Ma'anshan, Anhui 243002, P. R. China

† Electronic supplementary information (ESI) available. See <https://doi.org/10.1039/d2sc03375e>



**Scheme 1** Self-assembled Pt–Ru hybrid prodrug with multi-enzymatic activities (CAT, POD, and GPx) for manipulating redox homeostasis and chemo-catalytic synergistic therapy of hypoxic tumors.

have entered clinical trials (NAMI-A, TLD1433, *etc.*),<sup>31–33</sup> and ultrasmall ruthenium oxide nanoenzymes have recently been reported with catalase activity,<sup>34–37</sup> design of ruthenium hybrid platinum drugs may provide a tantalizing angle for efficient treatment of hypoxic tumors.

Herein, we developed a platinum(IV)–ruthenium hybrid prodrug, named as **Pt–Ru**, through a simple one-pot mixing step in water at room temperature. As shown in Scheme 1, ruthenium elements present mixed-valence states (Ru<sup>3+</sup> and Ru<sup>4+</sup>) and act as glues to bind Pt(IV) complexes together, and most importantly, endow this newly developed Pt(IV) prodrug with multi-enzymatic activities, that is, catalase (CAT) activity to generate O<sub>2</sub> *in situ*, peroxidase (POD) activity to produce ROS, and glutathione peroxidase (GPx) to deplete GSH. Therefore, **Pt–Ru** treatment can effectively alleviate tumor hypoxia and show much higher antitumor efficacy than cisplatin both *in vitro* and *in vivo*. This study suggests that endowing drugs with multi-enzyme activities to regulate tumor redox homeostasis will be a novel strategy for developing the next generation of platinum drugs.

## Results and discussion

### Fabrication of Pt–Ru hybrids

The detailed synthesis process of **Pt–Ru** hybrids is illustrated in Scheme 1. Initially, a Pt(IV) prodrug functionalized with succinic anhydride as the axial ligand was synthesized, named as Pt(IV)–COOH and characterized by <sup>1</sup>H NMR (Fig. S1, ESI†). Then **Pt–Ru** hybrids were fabricated *via* a simple and robust synthesis pathway under ambient conditions, where Pt(IV)–COOH, triethylamine and RuCl<sub>3</sub> were simply mixed in water and then

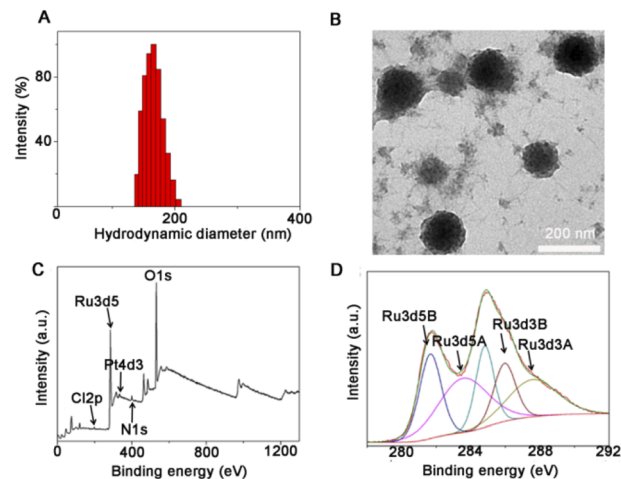


**Fig. 1** The morphology and composition of as-prepared Pt–Ru hybrids measured by (A) DLS; (B) TEM; (C and D) XPS of Pt–Ru.

stirred with FDA approved water-soluble polymers (PVP and F127) at room temperature. Herein, ruthenium acted as an adhesive to assemble Pt(IV) prodrugs into nanoparticles by reacting with carboxyl groups, meanwhile, the mixed-valence properties of Ru endow nanoparticles with multi-enzyme activity. Transmission electron microscopy (TEM) and dynamic laser scattering (DLS) experiments showed that **Pt–Ru** hybrids were well distributed in aqueous solution with uniform spherical morphology, and the average particle sizes were 160–180 nm (Fig. 1A and B). The X-ray photoelectron spectroscopy (XPS) survey spectrum showed that **Pt–Ru** hybrids contained Pt, Ru, N, O and Cl elements (Fig. 1C), and the molar ratio of Pt : Ru = 1 : 2 was also determined by ICP-MS (Table S1, ESI†). The high-resolution XPS spectrum (Fig. 1D) further confirmed the presence of mixed-valence states of the Ru element: the peak at 281.6 eV and 284.9 eV could be attributed to Ru<sup>3+</sup> and Ru<sup>4+</sup>, respectively,<sup>38</sup> while the presence of Pt<sup>4+</sup> was also verified by the XPS peak at 75.33 eV (Fig. S2, ESI†).<sup>39</sup> **Pt–Ru** hybrids exhibited excellent stability in water, PBS, 10% FBS for at least 5 days as indicated by the relatively stable hydrodynamic diameters (Fig. S3, ESI†). However, GSH (10 mM) could effectively promote the decomposition of **Pt–Ru** hybrids, as indicated by the gradually decreased DLS diameters from *ca.* 210 nm to 90 nm in 12 h (Fig. S4 and S5†, ESI). The drug release file of **Pt–Ru** in aqueous solution in the presence of GSH (1, 5 and 10 mM) was also monitored by ICP-MS. It is clear that GSH could promote the decomposition of **Pt–Ru**, and *ca.* 80% of Pt content could be released in 12 h, most likely in the form of cisplatin while only *ca.* 10% of Ru content was released under the same conditions (Fig. S6, ESI†). These data suggested that a high concentration of GSH in cancer cells could act as a reducing agent of **Pt–Ru** hybrids to release cisplatin.

### Multi-enzymatic activities of Pt–Ru hybrids

First, the CAT mimic activity of **Pt–Ru** hybrids was evaluated by monitoring the decomposition of H<sub>2</sub>O<sub>2</sub> to produce oxygen. As shown in Fig. 2A, the UV-visible absorbance of H<sub>2</sub>O<sub>2</sub> (10 mM)

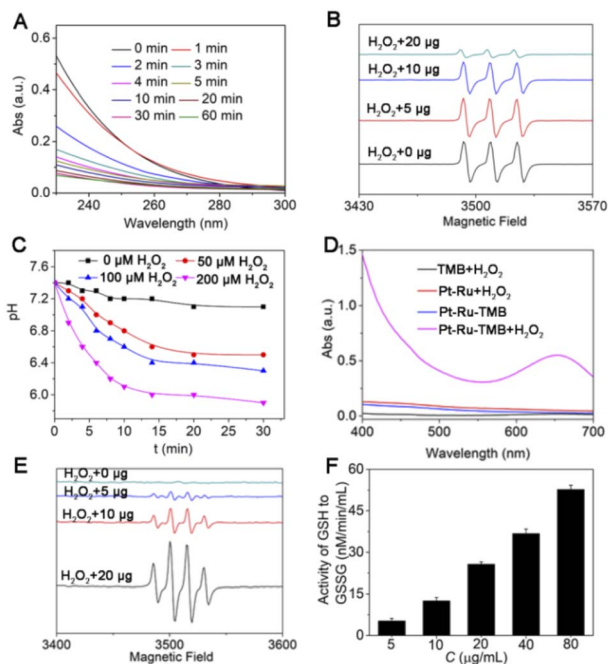


Fig. 2 (A) Consumption of  $\text{H}_2\text{O}_2$  over time in the presence of **Pt-Ru** (20  $\mu\text{g}$ ); effect of **Pt-Ru** at indicated doses on the (B) production of  $\text{O}_2$ ; (C) decrease of pH values; (D and E) generation of  $\cdot\text{OH}$ , respectively, in the presence of  $\text{H}_2\text{O}_2$ ; (F) effect of **Pt-Ru** on the production of GSSG from GSH.

was rapidly decreased in 5 min in the presence of **Pt-Ru** hybrids (20  $\mu\text{g}$ ), accompanied by bubble generation in the cuvette, indicating the rapid decomposition of  $\text{H}_2\text{O}_2$ . Meanwhile, the electron spin resonance (ESR) technique was employed to detect oxygen generation by using CTPO as an  $\text{O}_2$  trapping agent. As shown in Fig. 2B, CTPO had a characteristic triplet signal which was not affected by  $\text{H}_2\text{O}_2$  alone.

However, such a signal was gradually quenched by **Pt-Ru** hybrids in a dose-dependent manner (5–20  $\mu\text{g}$ ) in the presence of the same concentration of  $\text{H}_2\text{O}_2$ , indicating oxygen production mediated by **Pt-Ru** hybrids. Moreover, the pH value of the **Pt-Ru**/ $\text{H}_2\text{O}_2$  mixture solution gradually decreased with the progress of catalytic reaction, the more  $\text{H}_2\text{O}_2$ , the lower the pH value of the solution. For example, when the concentration of  $\text{H}_2\text{O}_2$  was 200  $\mu\text{M}$ , the pH value of the mixture solution decreased from 7.4 to 6.0 within 10 min, but only decreased to 6.8 when the  $\text{H}_2\text{O}_2$  concentration was 50  $\mu\text{M}$  (Fig. 2C). This further proved that **Pt-Ru** hybrids could simulate CAT activity by catalyzing  $\text{H}_2\text{O}_2$  to produce oxygen and protons. Second, the POD mimic activity of **Pt-Ru** hybrids was evaluated by monitoring the  $\cdot\text{OH}$  production from  $\text{H}_2\text{O}_2$ . Due to the high chemical activity and short lifetime of  $\cdot\text{OH}$ , a colorimetric indicator 3,3',5,5'-tetramethyl-benzidine (TMB) was employed, which could be oxidized by  $\cdot\text{OH}$  accompanied by a colorless-to-blue color change. As shown in Fig. 2D, the oxidation of TMB only occurred when **Pt-Ru** and  $\text{H}_2\text{O}_2$  were both present, as indicated by the emerging characteristic peak at 650 nm. The more  $\text{H}_2\text{O}_2$ , the more TMB oxidized, which verified the  $\cdot\text{OH}$  production from  $\text{H}_2\text{O}_2$  (Fig. S7, ESI†). Meanwhile, ESR spectroscopy was also employed using DMPO as an  $\cdot\text{OH}$  trapping

agent. With increasing amount of **Pt-Ru** hybrids (5–20  $\mu\text{g}$ ) in aqueous solution containing  $\text{H}_2\text{O}_2$ , a quadruplet ESR signal gradually emerged and increased, which was the characteristic peak of  $\cdot\text{OH}$  (Fig. 2E). These findings demonstrated the POD-mimic activity of **Pt-Ru** hybrids that could catalyze  $\text{H}_2\text{O}_2$  to produce  $\cdot\text{OH}$ .

In addition, the GPx mimic activity of **Pt-Ru** hybrids was evaluated using a GPx assay kit, and we found that the GSSG/GSH ratio gradually increased in **Pt-Ru** treated cells in a dose-dependent manner (Fig. 2F). This was consistent with the intrinsic activity of GPx that catalyzed the oxidation of GSH to oxidized glutathione (GSSG). These findings demonstrated the multi-enzymatic activities (CAT, POD, and GPx) of **Pt-Ru** hybrids in the presence of  $\text{H}_2\text{O}_2$ , which would be highly beneficial for regulating redox homeostasis.

### Redox homeostasis regulation and chemo-catalytic synergistic therapy

To verify the great potential of **Pt-Ru** hybrids in redox homeostasis regulation, *e.g.* alleviating hypoxia, enhancing oxidative stress and depleting GSH, we further investigated the catalytic behavior of **Pt-Ru** hybrids in living cells. Initially, the changes of intracellular  $\text{O}_2$  content were monitored by CLMS using RDDP ( $[\text{Ru}(\text{dpp})_3]\text{Cl}_2$ ) as the oxygen indicator, the fluorescence of which could be quenched by  $\text{O}_2$ .<sup>40</sup> As shown in Fig. 3A, the red fluorescence of RDDP in hypoxic cells was more intensive than that in normoxic cells, moreover, the fluorescence was remarkably quenched after **Pt-Ru** treatment (5  $\mu\text{M}$ , 24 h) while not affected by cisplatin, indicating an increased  $\text{O}_2$  content in **Pt-Ru** treated cells. Once the hypoxic cells were pretreated with NAC (a ROS scavenger) to remove intracellular  $\text{H}_2\text{O}_2$ , **Pt-Ru** treatment could not affect the fluorescence of RDDP either, further confirming that intracellular  $\text{H}_2\text{O}_2$  was the source of  $\text{O}_2$  in this case. Meanwhile, the immunofluorescence assay showed that the expression level of the hypoxia inducible factor (HIF-1 $\alpha$ ) in hypoxic MCF-7 cells was greatly reduced after **Pt-Ru** treatment (5  $\mu\text{M}$ , 24 h), as indicated by the quenched red fluorescence, but not affected by cisplatin at the same concentration (Fig. 3B). This demonstrated that **Pt-Ru** could alleviate tumor hypoxia by catalyzing endogenous  $\text{H}_2\text{O}_2$  to produce oxygen.

Then we monitored the changes of intracellular ROS and GSH levels induced by **Pt-Ru** hybrids. Confocal microscopy

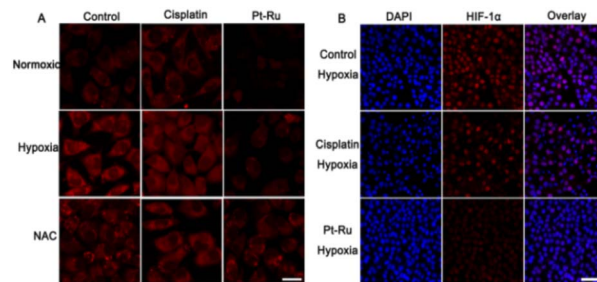


Fig. 3 CLSM images of (A)  $\text{O}_2$  content and (B) HIF-1 $\alpha$  expression in MCF-7 cells after 24 h treatment with cisplatin or **Pt-Ru** hybrids (5  $\mu\text{M}$ ). Scale bar = 20  $\mu\text{m}$  (A); 100  $\mu\text{m}$  (B).





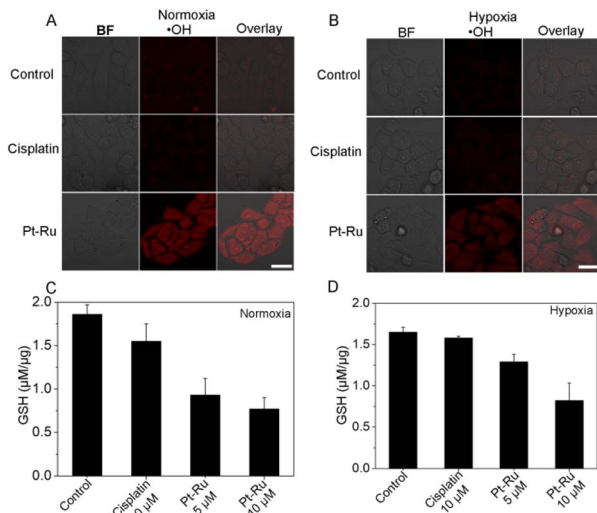


Fig. 4 (A and B) CLSM images of  $\cdot\text{OH}$  production and (C and D) GSH depletion in MCF-7 cells after incubation with cisplatin or **Pt-Ru** hybrids for 36 h under normoxia and hypoxia, respectively. Scale bar = 20  $\mu\text{m}$ .

showed that **Pt-Ru** treatment (5  $\mu\text{M}$ , 24 h) could induce substantial  $\cdot\text{OH}$  generation, as indicated by the emerging fluorescence from the  $\cdot\text{OH}$  specific probe, which was not observed in cisplatin treated cells under the same conditions (Fig. 4A and B). However, the generation of hydroxyl radicals was negligible once the cells were pre-treated with NAC (Fig. S8, ESI $^\dagger$ ). Meanwhile, flow cytometry showed that **Pt-Ru** treatment could induce intracellular ROS elevation in a dose-dependent manner (Fig. S9, ESI $^\dagger$ ). We also monitored the capability of **Pt-Ru** hybrids to produce  $\text{O}_2^{\cdot-}$  as cisplatin was known to activate nicotinamide adenine dinucleotide phosphate oxidases (NOXs) that could catalyze  $\text{O}_2$  into  $\text{O}_2^{\cdot-}$ . Confocal microscopy using dihydroethidium as an  $\text{O}_2^{\cdot-}$  specific probe showed that both cisplatin and **Pt-Ru** hybrids could induce  $\text{O}_2^{\cdot-}$  generation in hypoxic cells, the latter of which induced more, further confirming the hypoxia relief in **Pt-Ru** treated cells which provided more  $\text{O}_2$  as a substrate for NOX catalysis (Fig. S10, ESI $^\dagger$ ). Furthermore, the GSH assay showed that the GSH levels in normoxic and hypoxic MCF-7 cells after **Pt-Ru** treatment were both significantly lower than that in the untreated or cisplatin treated cells (C and D). This would be beneficial to minimize GSH-mediated cisplatin detoxification. These results demonstrated the intracellular catalytic activity of **Pt-Ru**

hybrids capable of simultaneously alleviating hypoxia, enhancing oxidative stress and depleting GSH.

Inspired by these redox homeostasis regulation capabilities, the anticancer activity of **Pt-Ru** hybrids was evaluated under both normoxia (21%  $\text{O}_2$ ) and hypoxia (1%  $\text{O}_2$ ) using a 48 h MTT assay.

Cisplatin-sensitive breast (MCF-7) and cisplatin-resistant human lung (A549R) carcinoma cell lines were selected and cisplatin was adopted as a positive control. As shown in Table 1 and Fig. S11 $^\dagger$  (ESI), **Pt-Ru** hybrids always exhibited higher anti-cancer activity than cisplatin whether under normoxic or hypoxic conditions, suggesting an effective chemo-catalytic synergistic therapy. Moreover, the toxicity of **Pt-Ru** against cancer cells under hypoxia was similar to that under normoxia, while that of cisplatin was substantially reduced under hypoxia. Take the A549R cell line as an example, when the  $\text{O}_2$  concentration was decreased from 21% to 1%, the  $\text{IC}_{50}$  value of **Pt-Ru** remained *ca.*  $19.3 \pm 2.4 \mu\text{M}$  while that of cisplatin increased from  $49.7 \pm 3.7 \mu\text{M}$  to  $65.2 \pm 3.1 \mu\text{M}$ , indicating the capability of **Pt-Ru** to overcome hypoxia and cisplatin resistance. It was worth mentioning that the cytotoxicity of **Pt-Ru** was substantially decreased in NAC-pretreated cells while the cytotoxicity of cisplatin was not affected by NAC at all. This was reasonable as NAC performed as an  $\text{H}_2\text{O}_2$  scavenger to diminish the substrate of catalysis reaction, thus inhibiting the catalytic activity of **Pt-Ru**.

Furthermore, the immunofluorescence assay using phosphorylated histone  $\gamma\text{-H2AX}$  as a DNA break marker also showed that **Pt-Ru** hybrids could trigger DNA damage effectively in both normoxic and hypoxic cells, and the effect was better than that of cisplatin under the same conditions (Fig. 5A). We also detected the distribution of **Pt-Ru** in living MCF-7 cells by ICP-MS (Fig. 5B). We found that the Pt content mainly distributes in the cytosol and nucleus while the Ru content mainly distributes in the cytosol and mitochondria. It was worth mentioning that after 36 h incubation the uptakes of **Pt-Ru** and cisplatin by MCF-7 cells were basically the same, but the cytotoxicity of **Pt-Ru** was *ca.* 3-fold higher than that of cisplatin, further verifying the chemo-catalytic synergistic therapy.

### In vivo antitumor efficacy

Finally, we evaluated the antitumor efficacy of **Pt-Ru** hybrids in nude mice bearing MCF-7 tumors, the initial volumes of which were *ca.*  $200 \text{ mm}^3$ . These mice were randomly divided into three groups ( $n = 3$ ) and intravenously injected (i.v. 100  $\mu\text{L}$ ) with PBS (control), cisplatin (5  $\text{mg kg}^{-1}$ ), and **Pt-Ru** (5  $\text{mg kg}^{-1}$ ), respectively, only on the 1<sup>st</sup> day. Then the tumor volumes were

Table 1  $\text{IC}_{50}$  ( $\mu\text{M}$ ) values of tested compounds towards different cell lines under normoxia and hypoxia, respectively<sup>a</sup>

Drug	MCF-7		NAC- pretreated MCF-7		A549R	
	Nor.	Hyp.	Nor.	Hyp.	Nor.	Hyp.
<b>Pt-Ru</b>	$2.80 \pm 0.38$	$4.83 \pm 0.42$	$5.40 \pm 0.62$	$10.04 \pm 0.76$	$11.63 \pm 0.85$	$19.30 \pm 2.40$
Cisplatin	$6.74 \pm 0.88$	$14.28 \pm 1.25$	$8.83 \pm 0.54$	$13.98 \pm 1.21$	$49.70 \pm 3.70$	$65.20 \pm 3.10$

<sup>a</sup> Data are presented as the means  $\pm$  standard deviations (SD) of three repeated measurements.



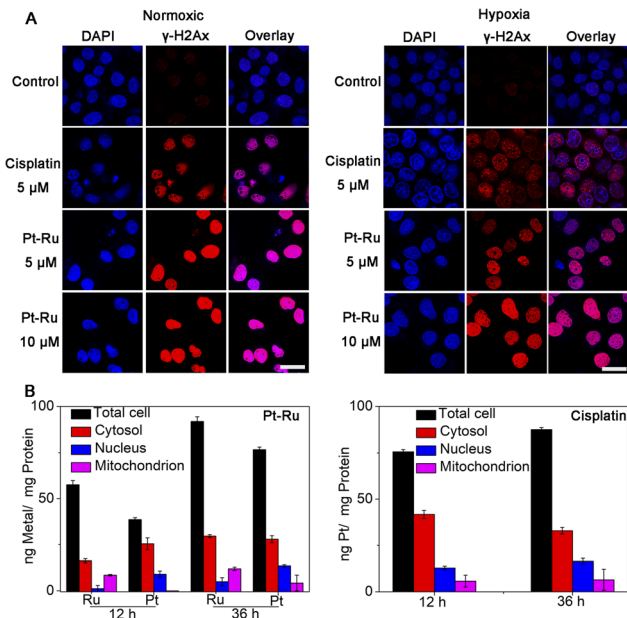


Fig. 5 (A) Immunofluorescence of  $\gamma$ -H2AX (DNA breaks foci) in MCF-7 cells, scale bar = 20  $\mu$ m; (B) distribution of Ru and Pt elements in MCF-7 cells after different incubation times with Pt-Ru and cisplatin (5  $\mu$ M), respectively.

measured every 3 days and all mice were sacrificed after 18 days for tumor collection. As shown in Fig. 6A and B, the tumor sizes in the control and cisplatin groups increased from 200 to 3280 and 1807  $\text{mm}^3$ , respectively, while Pt-Ru displayed much higher inhibitory activity against tumor growth where the tumor size only increased to 681  $\text{mm}^3$ . Meanwhile, Pt-Ru treated mice did

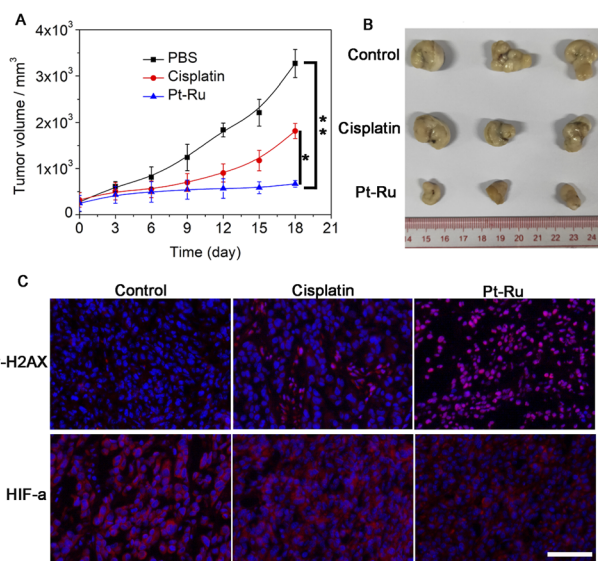


Fig. 6 *In vivo* anti-tumor efficacy of PBS, cisplatin and Pt-Ru hybrids investigated following intravenous (i.v.) injection at a dose of 5  $\text{mg kg}^{-1}$  or cisplatin-equivalent dose of 5  $\text{mg kg}^{-1}$ . (A) Changes in MCF-7 tumor volumes; (B) image of resected tumors; (C) expression of DNA damage marker ( $\gamma$ -H2AX) and HIF-1 $\alpha$  in tumor tissues after 96 h of Pt-Ru hybrid treatment (5  $\text{mg kg}^{-1}$ , i.v.). Scale bar = 100  $\mu$ m.

not show obvious body weight loss while cisplatin caused 16% of weight loss during treatment, indicating minimum side effects (Fig. S12, ESI†). The immunofluorescence assay showed that Pt-Ru hybrids induced substantial DNA damage as indicated by the up-regulated  $\gamma$ -H2AX, as well as significant inhibition of HIF-1 $\alpha$  expression in tumors tissues, the effect of which was much more apparent than that in the cisplatin group (Fig. 6C). These results demonstrated that Pt-Ru hybrids had excellent *in vivo* anti-tumor efficacy with hypoxia relieving capability.

## Conclusions

In summary, we developed a Pt-Ru hybrid prodrug with multi-enzymatic activities (CAT, POD, and GPx) for efficient chemocatalytic synergistic therapy of hypoxic tumors. The catalytic properties were mainly attributed to the ruthenium hybridization which endowed the novel Pt(IV) prodrug with redox homeostasis regulation capability, that is, alleviating hypoxia, producing excess ROS and depleting GSH simultaneously, which led to a superior therapeutic efficacy to cisplatin both *in vitro* and *in vivo*. This work suggested that endowing the drugs with multi-enzymatic activities would be a promising strategy for developing the next generation of platinum drugs.

## Experimental section

### Materials

Cisplatin and  $\text{RuCl}_3$  were both purchased from Bidepharm. Pluronic F-127 (F127, molecular weight = 10 000  $\text{g mol}^{-1}$ ) was bought from Macklin reagent company. Succinic anhydride, 3,3',5,5'-tetramethylbenzidine (TMB) and triethylamine were both purchased from Aladdin reagent company. 3-(4,5-Dimethylthiazol-2-yl)-2,5-diphenyltetrazolium bromide (MTT) was supplied by Sigma USA. Distilled water was purified by passing through a Millipore Milli-Q Biocel purification system (18.2 M $\Omega$ ) with a 0.22  $\mu$ m filter.

### General instruments

UV-Vis spectra were monitored with a Varian Cary 100 UV/vis spectrophotometer (USA). Ru and Pt contents were measured on a Thermo X Series 2 Inductively Coupled Plasma Mass Spectrometer (Thermo Fisher Corp., USA). Transmission Electron Microscopy (T12, FEI Tecnai G2 Spirit, Holland) was performed at room temperature. Dynamic light scattering (DLS) studies were performed using a Zetasizer Nano instrument (EliteSizer, Bruker, Germany). The ruthenium and platinum contents were determined using an iCAP RQ. X-ray photoelectron spectra (XPS) were recorded on an S-Probe XPS spectrometer with Al K $\alpha$  radiation as the X-ray source (1486 eV). Cell imaging experiments were carried out on a confocal microscope (Zeiss LSM-710/800, ZEISS, Germany). Flow cytometric analysis was done using a BD FACS Calibur™ flow cytometer (Becton Dickinson, USA).



### Synthesis of $[\text{Pt}(\text{NH}_3)_2\text{Cl}_2(\text{O}_2\text{CCH}_2\text{CH}_2\text{CO}_2\text{H})_2]$

The complex  $c,c,t$ - $[\text{Pt}(\text{NH}_3)_2\text{Cl}_2(\text{OH})_2]$  was synthesized by literature methods.<sup>41</sup> Synthesis of  $[\text{Pt}(\text{NH}_3)_2\text{Cl}_2(\text{O}_2\text{CCH}_2\text{CH}_2\text{CO}_2\text{H})_2]$  was carried out according to a previous report.<sup>42</sup> Succinic anhydride (0.18 g, 1.8 mM) was added to a solution of  $c,c,t$ - $[\text{Pt}(\text{NH}_3)_2\text{Cl}_2(\text{OH})_2]$  (0.2 g, 0.6 mM) in dimethyl sulfoxide (DMSO, 5 mL). Then this solution was stirred at room temperature for 24 h under dark conditions. After the reaction, the solution was filtered and the precipitate was discarded, and then ultrapure water was added to the filtrate, followed by freeze-drying. A small amount of acetone was added to the lyophilized product for washing, and then the product was washed with ether and a small amount of methanol, obtaining the white product.

### Fabrication of Pt–Ru nanoparticles

**Pt–Ru** nanoparticles were prepared by aqueous synthesis at room temperature. First,  $[\text{Pt}(\text{NH}_3)_2\text{Cl}_2(\text{O}_2\text{CCH}_2\text{CH}_2\text{CO}_2\text{H})_2]$  (50 mg, 0.093 mM) was added to a 50 mL eggplant bottle and then 20 mL of water was added. This solution was stirred for 30 min at room temperature. Next 20  $\mu\text{L}$  triethylamine was added slowly to the aqueous solution and stirred for 24 h. 20 mg  $\text{RuCl}_3$  was added to the above solution, and the solution was continuously stirred for 12 h, and then 10 mL of 50 mg F127 and 20 mg PVP solution was added, followed by continuous stirring for 12 h. The final product was obtained by centrifuging and washing with water. The contents of Ru and Pt in the product were determined by ICP-MS.

### Effect of glutathione on the stability of Pt–Ru nanoparticles

20  $\mu\text{g mL}^{-1}$  of **Pt–Ru** was dispersed in glutathione solution (5, 10 mM) and then incubated at 37 °C for 0, 1, 4, 12, 24 and 48 h respectively. The hydrodynamic diameter of **Pt–Ru** nanoparticles was measured at the above time. The stability of the nanoparticles was measured with 3 mL of water, PBS and 10% FBS water solution, and then, the particle size change of nanoparticles was measured every day for a total of 5 days.

### Drug release study

0.5 mL of the **Pt–Ru** solution was transferred to a dialysis device (MWCO 8000–14000, Spectrum) that was immersed in pH 7.4 and 5.0 buffer solution and the GSH groups contained different concentrations of GSH (1, 5, 10 mM). After placing at 37 °C for 48 h, the Pt and Ru elements were examined by ICP-MS. The cumulative release of the Pt and Ru elements was calculated as follows:  $M \text{ release } (\%) = (M_c/M_0) \times 100\%$ , where  $M_c$  is the amount of Ru or Pt released from **Pt–Ru** at time  $t$  and  $M_0$  is the amount of Ru or Pt elements in the **Pt–Ru**.

### Decomposition of $\text{H}_2\text{O}_2$ by Pt–Ru and production of $\text{O}_2$

$\text{H}_2\text{O}_2$  has UV-vis absorption at 240 nm, so the UV absorption was measured at 240 nm after the reaction to calibrate the concentration of  $\text{H}_2\text{O}_2$ . First, **Pt–Ru** (20  $\mu\text{g mL}^{-1}$ ) was added to water solutions containing  $\text{H}_2\text{O}_2$  (10 mM) at 37 °C. After incubation for different time intervals, the UV/Vis spectra of the

residual  $\text{H}_2\text{O}_2$  were recorded. The production of  $\text{O}_2$  from the reaction of  $\text{H}_2\text{O}_2$  (1 mM) with different concentrations of **Pt–Ru** (20  $\mu\text{g}$ ) at 37 °C was detected by EPR measurements using the oxygen-sensitive spin-label probe CTPO (0.1 mM). The EPR spectra were recorded on a Bruker A300 X-band EPR spectrometer. The change of pH in the reaction process was measured with a handheld pH meter for a total of 30 minutes.

### POD mimic activity of Pt–Ru

To investigate the POD mimic activity, different concentrations of TMB and  $\text{H}_2\text{O}_2$  with **Pt–Ru** (20  $\mu\text{g mL}^{-1}$ ) were combined at room temperature for 10 min in water solutions. The absorbance of TMB (650 nm) was recorded after 30 min of reaction time. The  $\cdot\text{OH}$  was also monitored using the DMPO adduct in the EPR spectrometer.

### Cell culture conditions

MCF-7 cells were obtained from the Experimental Animal Center of Sun Yat-Sen University (Guangzhou, China), and then maintained in DMEM medium containing 10% FBS, streptomycin (100  $\mu\text{g mL}^{-1}$ ) and penicillin (100 U  $\text{mL}^{-1}$ ). A549R cells were purchased from Shanghai Zhong Qiao Xin Zhou Biotechnology Co. Ltd, and then maintained in 1640 medium containing 10% FBS, 20  $\mu\text{M}$  Cisplatin streptomycin (100  $\mu\text{g mL}^{-1}$ ) and penicillin (100 U  $\text{mL}^{-1}$ ). These cells were cultured in a humidified incubator in an atmosphere of 5%  $\text{CO}_2$  and 95% air at 37 °C. Hypoxic culture: cells were maintained at 37 °C in a humidified atmosphere containing 1% oxygen, 5% carbon dioxide and 94% nitrogen. Simulated hypoxic culture: 100  $\mu\text{M}$   $\text{CoCl}_2$  solution was used to simulate the hypoxia conditions according to ref. 17.

### Cell uptake experiment and distribution

MCF-7 cells were seeded in a 10 cm dish and incubated for 24 h, and then treated with cisplatin and **Pt–Ru** (5  $\mu\text{M}$ ) for 12 h and 36 h. Then, the cells were washed three times with PBS and then the cells were collected and divided into three groups. The mitochondria and nucleus were extracted using a mitochondria extraction kit (Mitochondria Isolation Kit for Cell and Tissue, Yeasen Biotech) and nucleus extraction kit (Sangon Biotech (Shanghai) Co., Ltd) for the two groups of cells. The mitochondria, nucleus and another cell were added to a cell lysis buffer respectively to extract proteins. Then, a BCA protein quantification kit was used to quantify the protein. The Ru and Pt elements in the proteins were determined by ICP-MS.

### Generation of $\text{O}_2$ in MCF-7 cells

MCF-7 cells ( $1 \times 10^5$ ) were seeded into culture dishes and incubated at 37 °C for 12 h. Then, all those cells were incubated with  $[\text{Ru}(\text{dpp})_3]_2\text{Cl}_2$  (0.1  $\mu\text{M}$  in DMEM medium) for another 4 h, and then each dish was rinsed with PBS three times and further incubated with **Pt–Ru** solutions for 24 h. The cells with *N-Acetyl-L-cysteine* (NAC, hydrogen peroxide scavenging reagent) treatment were used for study and the cells without treatment served as the control. Finally, all those cells were washed with





DMEM medium three times and then captured using a CLSM under excitation at 488 nm; the emission was collected between 600 and 640 nm.

#### HIF-1 $\alpha$ expression measured by immunofluorescence

After subculture, MCF-7 cells were laid in 12 well plates, and cell climbing sheets were placed in each hole of the plates in advance. Firstly, CoCl<sub>2</sub> solutions were added into each well, and then **Pt-Ru** and cisplatin were added and the cells were incubated for 24 h. The cells were fixed with a 4% paraformaldehyde solution and permeabilized using 1% Triton X-100. After incubation with a blocking buffer (1  $\times$  PBS, 0.1% goat serum, 0.075% glycine) for 1 h at room temperature, the primary rabbit polyclonal antibody for HIF-1 $\alpha$  was added and the cells were incubated at 4  $^{\circ}$ C for 24 h. The cells were then incubated with the secondary Alexa Fluor 488 goat anti-rabbit antibody for 4 h at 37  $^{\circ}$ C. After washing three times with PBS, the cells were captured using a confocal microscope (LSM 800, Carl Zeiss, Germany). Emission was collected at 520 nm on excitation at 488 nm.

#### MTT assay

MCF-7 and A549R cells were plated in 96 well plates. After 24 h of culture, different concentrations of cisplatin and **Pt-Ru** were added for 44 h incubation, and then MTT was added for another 4 h of incubation. For cytotoxicity under hypoxia, the cells should better be adapted to hypoxia 1 week in advance. Other experimental methods are the same as those under normal oxygen. Then the medium was removed and 150  $\mu$ L of DMSO was added to each well. The cell viability was evaluated by measuring the absorbance at 595 nm (Infinite F200, Tecan, Switzerland).

#### Determination of intracellular ROS levels

MCF-7 cells were treated with different concentrations of **Pt-Ru** for 24 h. For the cells in the hypoxia group, a cobalt chloride solution was added at the same time, and other operations were the same as those in the normoxia group. Then, the cells were stained with 10  $\mu$ M DCFH-DA for 20 min at 37  $^{\circ}$ C. After washing with PBS three times, the green fluorescence intensity of DCFH-DA was detected by flow cytometry.

#### Detection of hydroxyl radicals ( $\cdot$ OH) and superoxide anions ( $O_2^{\cdot-}$ ) in cells

MCF-7 cells were seeded in a 35 mm dish and incubated for 24 h, and then treated with different concentrations of cisplatin and **Pt-Ru** for 36 h. The cells in the hypoxia group were treated with a cobalt chloride solution at the same time, and other operation methods were the same. Then, the cells were washed three times with PBS and then treated with a hydroxyl radical probe (hydroxyphenyl fluorescein, HPF) and superoxide anion probe (dihydroethidium, DHE) for 20 min. For the NAC group, 0.1 mM of NAC solution was added 2 h before dosing. After washing three times with PBS, the cells were captured using a confocal microscope (LSM 800, Carl Zeiss, Germany). Emission was collected at 520 nm on excitation at 488 nm.

#### Detection of intracellular GSH levels

The intracellular GSH level was measured using a GSH Assay Kit (Beyotime, China). MCF-7 cells were seeded in a 10 cm dish and incubated for 24 h, and then treated with different concentrations of cisplatin and **Pt-Ru** for 36 h. The cells were washed three times with PBS and centrifuged with a cell lysate to collect the supernatant. The absorption was recorded at 414 nm on an Infinite M200 pro microplate reader.

#### $\gamma$ -H2AX expression measured by immunofluorescence

After subculture, MCF-7 cells were placed in 12 well plates. After incubation for 24 h, cisplatin and the drug were added respectively, and then the cells were incubated for 36 h. For the hypoxic group, a cobalt chloride solution was added while adding drugs. These cells were then fixed with 4% paraformaldehyde solution and permeabilized using 1% Triton X-100. After incubation with a blocking buffer (1  $\times$  PBS, 0.1% goat serum, 0.075% glycine) for 1 h at room temperature. The primary rabbit polyclonal antibody for  $\gamma$ -H2AX (2.5  $\mu$ g mL<sup>-1</sup> in blocking buffer) was added and the cells were incubated at 4  $^{\circ}$ C for 12 h. The cells were then incubated with the secondary Alexa Fluor 488 goat anti-rabbit antibody for 1 h at 37  $^{\circ}$ C. The cells were incubated with DAPI for 20 min at 37  $^{\circ}$ C. After washing three times with PBST (PBS with 1% Triton X-100), the cells were visualized using a confocal microscope (LSM 800, Carl Zeiss, Germany). For  $\gamma$ -H2AX, emission was collected at 520 nm upon excitation at 488 nm, and for DAPI, emission was collected at 470 nm on excitation at 405 nm.

#### *In vivo* anti-tumor therapy

All of the animal experiments were approved by the university animal care and use committee of Sun Yat-Sen University.

The female BALB/c-(nu/nu) nude mice aged 4–5 weeks were bought from Beijing Vitalriver Experimental Animal Technology Co. Ltd, under approval by Sun Yat-sen university laboratory animal center. All procedures used in this experiment were compliant with the local animal ethics committee. MCF-7 cells ( $2 \times 10^6$ ) were subcutaneously injected into the female mice. When the tumors grew to 200 mm<sup>3</sup>, those mice were divided into three groups and administered with an intravenous injection of PBS, cisplatin and **Pt-Ru**, respectively, on the 1<sup>st</sup> day. The tumor size was obtained using a Vernier caliper and the mice weight was measured every three days. The tumor volume was calculated by the formula:  $V = a^2 \times b/2$ , where  $a$  and  $b$  are the shortest and longest diameter of tumors. After 18 days of treatment, the mice were sacrificed and the major organs were collected for the enzyme linked immunosorbent assay (ELISA, Servicebio technology, Wuhan, China).

#### Statistical analysis

The significance of several experimental results was analyzed by using the analysis of variance (ANOVA) test. Probabilities  $p < 0.05$  (\*) and  $p < 0.002$  (\*\*), \*\*\* $p < 0.001$  were marked in figures and 0.05 was chosen as the significance level.



## Author contributions

G. G. Y. synthesized and fully characterized all materials, and also did the animal experiment. B. B. L. performed the ICP-MS for the revised manuscript. Experimental data collection and analysis by X. X. S. and Z. Y. P. Q. C. designed the work and drafted the manuscript. Z. W. M. gave revision suggestions and writing guidance for the paper.

## Conflicts of interest

There are no conflicts to declare.

## Acknowledgements

This work was financially supported by the National Natural Science Foundation of China [21837006, 91953117, and 22177141], Natural Science Foundation of Guangdong Province [2021A1515010342], Science and Technology Program of Guangzhou [202201011718], and Fundamental Research Funds for Central Universities.

## Notes and references

- 1 B. Yang, Y. Chen and J. Shi, *Adv. Mater.*, 2019, **31**, 1901778.
- 2 W. Wu, Y. Pu and J. Shi, *Adv. Sci.*, 2021, **8**, 2002816.
- 3 B. Yang, L. Ding, H. Yao, Y. Chen and J. Shi, *Adv. Mater.*, 2020, **32**, 1907152.
- 4 W. Wu, Y. Pu, X. Lu, H. Lin and J. Shi, *Adv. Healthcare Mater.*, 2021, **10**, 2001819.
- 5 X. Wang, X. Wang, S. Jin, N. Muhammad and Z. Guo, *Chem. Rev.*, 2019, **119**, 1138–1192.
- 6 M. Huo, L. Wang, Y. Chen and J. Shi, *Nat. Commun.*, 2017, **8**, 1–12.
- 7 M. L. Drakes and P. J. Stiff, *Cancers*, 2018, **10**, 302–322.
- 8 J. Chen, Y. Zhu, C. Wu and J. Shi, *Chem. Soc. Rev.*, 2020, **49**, 9057–9094.
- 9 Y. Da I, C. Xu, X. Sun and X. Chen, *Chem. Soc. Rev.*, 2017, **46**, 3830–3852.
- 10 C. C. Huang, W. T. Chia, M. F. Chung, K. J. Lin, C. W. Hsiao, C. Jin, W. H. Lim, C. C. Chen and H. W. Sung, *J. Am. Chem. Soc.*, 2016, 5222–5225.
- 11 Y. You, Z. Zhao, L. He, Z. Sun, D. Zhang, C. Shi, Q. Cheng, Y. Liu, L. Luo and T. Chen, *Adv. Funct. Mater.*, 2020, **30**, 2002369.
- 12 X. Zhu, Y. Gong, Y. Liu, C. Yang and X. Qin, *Biomaterials*, 2020, **242**, 119923.
- 13 C. Imberti, F. Lermyte, E. P. Friar, P. B. O'Connor and P. J. Sadler, *Chem. Commun.*, 2021, **57**, 7645–7648.
- 14 H. Shi, C. Imberti, G. J. Clarkson and P. J. Sadler, *Inorg. Chem. Front.*, 2020, **7**, 3533–3540.
- 15 J. Karges, T. Yempala, M. Tharaud, D. Gibson and G. Gasser, *Angew. Chem., Int. Ed.*, 2020, **59**, 7069–7075.
- 16 T. C. Johnstone, K. Suntharalingam and S. J. Lippard, *Chem. Rev.*, 2016, **116**, 3436–3486.
- 17 Q. Cao, D.-J. Zhou, Z.-Y. Pan, G.-G. Yang, H. Zhang, L.-N. Ji and Z.-W. Mao, *Angew. Chem., Int. Ed.*, 2020, **59**, 18556–18562.
- 18 Y. Yang, Y. Yu, H. Chen, X. Meng, W. Ma, M. Yu, Z. Li, C. Li, H. Liu, X. Zhang, H. Xiao and Z. Yu, *ACS Nano*, 2020, **14**, 13536–13547.
- 19 P. A. Ma, H. Xiao, C. Yu, J. Liu, Z. Cheng, H. Song, X. Zhang, C. Li, J. Wang, Z. Gu and J. Lin, *Nano Lett.*, 2017, **17**, 928–937.
- 20 H. Chen, J. Tian, W. He and Z. Guo, *J. Am. Chem. Soc.*, 2015, **137**, 1539–1547.
- 21 J. Liu, Q. Chen, L. Feng and Z. Liu, *Nano Today*, 2018, **21**, 55–73.
- 22 Q. Chen, L. Feng, J. Liu, W. Zhu, Z. Dong, Y. Wu and Z. Liu, *Adv. Mater.*, 2016, **28**, 7129–7136.
- 23 X. Fan, F. Yang, C. Nie, L. Ma, C. Cheng and R. Haag, *Adv. Mater.*, 2021, **33**, 2100637.
- 24 X. Xiao, S. Liang, Y. Zhao, M. Pang, P. a. Ma, Z. Cheng and J. Lin, *Biomaterials*, 2021, **277**, 121120.
- 25 G.-G. Yang, Z.-Y. Pan, D.-Y. Zhang, Q. Cao, L.-N. Ji and Z.-W. Mao, *ACS Appl. Mater. Interfaces*, 2020, **12**, 43444–43455.
- 26 H. Zhang, Y. Zhang, J. Cao, L. Ma and T. Chen, *Chem. Commun.*, 2022, **58**, 3759–3762.
- 27 M. Xu, B. Xue, Y. Wang, D. Wang, D. Gao, S. Yang, Q. Zhao, C. Zhou, S. Ruan and Z. Yuan, *Small*, 2021, **17**, 2101397.
- 28 L. Tong, C.-C. Chuang, S. Wu and L. Zuo, *Cancer Lett.*, 2015, **367**, 18–25.
- 29 C. Nathan and A. Cunningham-Bussell, *Nat. Rev. Immunol.*, 2013, **13**, 349–361.
- 30 S. Kwon, H. Ko, D. G. You, K. Kataoka and J. H. Park, *Acc. Chem. Res.*, 2019, **52**, 1771–1782.
- 31 S. Thota, D. A. Rodrigues, D. C. Crans and E. J. Barreiro, *J. Med. Chem.*, 2018, **61**, 5805–5821.
- 32 F. Heinemann, J. Karges and G. Gasser, *Acc. Chem. Res.*, 2017, **50**, 2727–2736.
- 33 M. Rausch, P. J. Dyson and P. Nowak-Sliwinska, *Adv. Therap.*, 2019, **2**, 1900042.
- 34 Z. Liu, L. Xie, K. Qiu, X. Liao, T. W. Rees, Z. Zhao, L. Ji and H. Chao, *ACS Appl. Mater. Interfaces*, 2020, **12**, 31205–31216.
- 35 C. Wu, X. Han, W. Feng, Z. Liu, L. Chen, B. Zhou, Y. Chen and J. Shi, *Chem. Eng. J.*, 2021, **411**, 128543.
- 36 H. Deng, W. Shen, Y. Peng, X. Chen, G. Yi and Z. Gao, *Chem.–Eur. J.*, 2012, **18**, 8906–8911.
- 37 S.-B. He, P. Balasubramanian, Z.-W. Chen, Q. Zhang, Q.-Q. Zhuang, H.-P. Peng, H.-H. Deng, X.-H. Xia and W. Chen, *ACS Appl. Mater. Interfaces*, 2020, **12**, 14876–14883.
- 38 X. Zhu, X. Chen, Z. Jia, D. Huo, Y. Liu and J. Liu, *J. Colloid Interface Sci.*, 2021, **603**, 615–632.
- 39 E. Ruggiero, J. Hernández-Gil, J. C. Mareque-Rivas and L. Salassa, *Chem. Commun.*, 2015, **51**, 2091–2094.
- 40 W. Zhen, Y. Liu, L. Lin, J. Bai, X. Jia, H. Tian and X. Jiang, *Angew. Chem., Int. Ed.*, 2018, **57**, 10309–10313.
- 41 M. Hall, C. Dillon, M. Zhang, P. Beale, Z. Cai, B. Lai, A. J. Stampfl and T. Hambley, *J. Biol. Inorg. Chem.*, 2003, **8**, 726–732.
- 42 K. R. Barnes, A. Kutikov and S. J. Lippard, *Chem. Biol.*, 2004, **11**, 557–564.

